ACES Asian Chemical Editorial Society

DOI: 10.1002/asia.201600771

CHEMISTRY AN ASIAN JOURNAL Communication

Photochemistry

Room-Temperature and Aqueous-Phase Synthesis of Plasmonic Molybdenum Oxide Nanoparticles for Visible-Light-Enhanced Hydrogen Generation

Jiayuan Shi,[a, b] Yasutaka Kuwahara,[a, c] Meicheng Wen,[a] Miriam Navlani-García,[a] Kohsuke Mori,[a, c] Taicheng An,[b, d] and Hiromi Yamashita*[a, c]

Abstract: A straightforward aqueous synthesis of MoO_{3-x} nanoparticles at room temperature was developed by using $(NH_4)_6Mo_7O_{24}{\cdot}4H_2O$ and $MoCl_5$ as precursors in the absence of reductants, inert gas, and organic solvents. SEM and TEM images indicate the as-prepared products are nanoparticles with diameters of 90–180 nm. The diffuse reflectance UV-visible-near-IR spectra of the samples indicate localized surface plasmon resonance (LSPR) properties generated by the introduction of oxygen vacancies. Owing to its strong plasmonic absorption in the visible-light and near-infrared region, such nanostructures exhibit an enhancement of activity toward visible-light catalytic hydrogen generation. MoO_{3-x} nanoparticles synthesized with a molar ratio of Mo^{VI}/Mo^{V} 1:1 show the highest yield of H_2 evolution. The cycling catalytic performance has been investigated to indicate the structural and chemical stability of the as-prepared plasmonic MoO_{3-x} nanoparticles, which reveals its potential application in visible-light catalytic hydrogen production.

With the aggravation of the global energy crisis and increasing ecological concerns about fossil fuel combustion, exploiting alternative and sustainable energies has become one of the crucial development strategies in many countries. As a type of abundant, clean, and renewable energy source, solar energy is viewed as the promising energy supply in the 21st century.[1] Moreover, hydrogen is proposed as an ideal energy carrier and has attracted widespread attention throughout the world.[2] During the past few years, great efforts have been made to achieve hydrogen production with solar energy by using various strategies including solar-driven water splitting, photo-biological hydrogen production, and photocatalytic hydrogen production; however, the spectrum range of light able to be exploited to drive the photocatalytic reaction has been limited.[3] Plasmonic-induced photocatalysis has been proposed to improve the efficiency of solar light absorption and solar energy conversion.[4] So far, the most extensively studied plasmonic nanostructures have been noble metals, such as Au and Ag, with excellent optical properties related to their localized surface plasmon resonance (LSPR) in a wide spectrum range from the visible-light region to the near infrared (NIR).[5] The LSPRs of metal nanostructures arise from the collective oscillation of the conduction electrons at the material surface, which holds great potential for developing various photocatalytic hydrogen-producing systems including metal–semiconductor composites, bimetals, and carbon-supported metal catalysts.[6] However, the earth rarity, high-cost, and inherent limitations (e.g., the rapid oxidation of Ag) of noble-metal-based nanomaterials restrict their large-scale practical applications.[7]

Recently, there have been reports on nonmetallic nanostructures with LSPR properties, which brings new opportunities of fabricating novel low-cost plasmonic photocatalysts.[8] For example, metal oxide semiconductors doped with heterovalent atoms (In-doped CdO, Al-doped ZnO, and Sb-doped SnO_2),[9] Cu-deficient chalcogenides ($Cu_{2-x}S$, $Cu_{2-x}Se$, and $Cu_{2-x}Te$),[10] and O-deficient transition-metal oxides (TiO_{2-x}, WO_{3-x}, and MoO_{3-x})[11] are known to exhibit strong LSPR absorbance and their LSPR tunability can be achieved by altering the stoichiometric compositions or adjusting dopant concentrations. For the fabrication of O-deficient metal oxides, hydrothermal reaction at high temperature and pressure are usually adopted, in which reductants (e.g., ascorbic acid, oleylamine, or ethanol) or inert gas (e.g., Ar) are always needed to prevent the complete oxidation of transition metals and to endow the resultant metal oxides with variable valence character. Clearly, a non-oxidative environment in the hydrothermal reaction is of vital importance for stabilizing the low-valent metal ions in the oxides

[a] Dr. J. Shi, Dr. Y. Kuwahara, Dr. M. Wen, Dr. M. Navlani-García, Dr. K. Mori, Prof. H. Yamashita
Graduate School of Engineering
Osaka University, Osaka 565-0871 (Japan)
E-mail: yamashita@mat.eng.osaka-u.ac.jp

[b] Dr. J. Shi, Prof. T. An
State Key Laboratory of Organic Geochemistry and Guangdong Key Laboratory of Environmental Protection and Resources Utilization
Guangzhou Institute of Geochemistry
Chinese Academy of Sciences, Guangzhou 510640 (China)

[c] Dr. Y. Kuwahara, Dr. K. Mori, Prof. H. Yamashita
Unit of Elements Strategy Initiative for Catalysts & Batteries (ESICB)
Kyoto University, Katsura, Kyoto 615-8520 (Japan)

[d] Prof. T. An
School of Environmental Science and Engineering
Guangdong University of Technology
Guangzhou 510006 (China)

Supporting information for this article can be found under http://dx.doi.org/10.1002/asia.201600771.

that increases the complexity and uncontrollability of the synthetic process.

In this work, we present a straightforward aqueous synthesis of MoO_{3-x} nanoparticles under non-heating conditions by using $(NH_4)_6Mo_7O_{24}{\cdot}4H_2O$ and $MoCl_5$ as precursors in the absence of reductants, inert gas, and organic solvents. The obtained MoO_{3-x}-Y (Y represents the Mo^{VI}/Mo^{V} molar ratio) nanostructures exhibit a strong LSPR response under visible-light irradiation. The morphology evolution and the LSPR tunability of the molybdenum oxide nanostructures were investigated with the change of molar ratio between Mo^{VI} from $(NH_4)_6Mo_7O_{24}{\cdot}4H_2O$ and Mo^{V} from $MoCl_5$. Moreover, we found that the obtained MoO_{3-x}-Y exhibited high activity for hydrogen evolution from ammonia borane (NH_3BH_3) under visible-light irradiation. Owing to the low-cost, easy operation of this method, and excellent photocatalytic activity of the resultant nanomaterials, the photocatalytic system shown in this work would be applicable for solar-light-driven hydrogen production.

The MoO_{3-x}-Y nanoparticles were prepared at room temperature by mixing two kinds of molybdenum salts with different valence states of Mo and then stirring for 48 hours in aqueous solution (see the Supporting Information). The obtained MoO_{3-x}-50 product exhibits a deep blue color that is clearly different from the white MoO_3 (Figure 1a). The coloration of

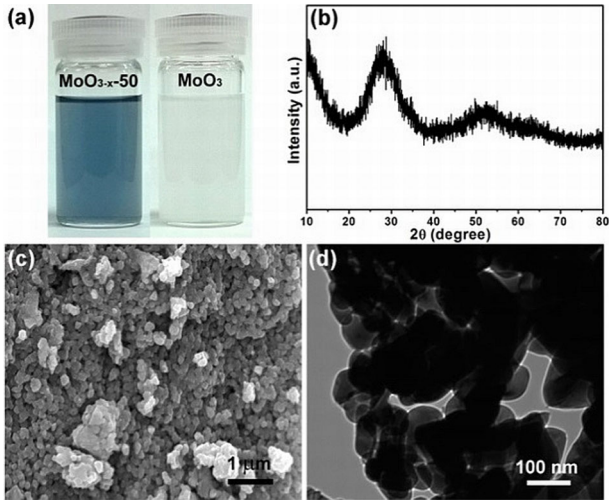

Figure 1. a) A photograph of the prepared MoO_{3-x}-50 and the commercial MoO_3 dispersed in ethanol. b) XRD pattern of MoO_{3-x}-50. c) FE-SEM and d) TEM images of MoO_{3-x}-50.

MoO_{3-x}-Y is mainly due to the presence of oxygen vacancies, which are associated with the coexistence of Mo^{V} and Mo^{VI} in the O-deficient oxides.[11c,d] The prepared blue samples are very stable in air and their original color does not fade away over several months. Figure 1b shows the XRD pattern of MoO_{3-x}-50. The product is mainly amorphous, which is associated with the room-temperature preparation of the nanoparticles, excluding the possibility of the formation of crystalline molybdenum oxides such as MoO_3 and Mo_2O_5. Field-emission scanning electron microscopy (FE-SEM) and transmission electron microscopy (TEM) images of the as-prepared MoO_{3-x}-50 indicate the product is in the shape of nanoparticles with diameters of 90–180 nm (Figure 1c and d). The formation of MoO_{3-x}-Y nanoparticles could be attributed to the strong interaction between the dissoluble Mo^{VI} and Mo^{V} species in strongly acidic medium (see the Supporting Information). Thermogravimetric analysis of MoO_{3-x}-50 indicated that the product is partially hydroxylated, but could be strongly considered as a molybdenum oxide compound (see the Supporting Information).

Figure 2a shows the diffuse reflectance UV-visible-NIR spectra of the as-prepared MoO_{3-x}-50 and commercial MoO_3. Both samples have signal responses in the UV region (200–450 nm), which is determined by the bandgap of MoO_3 (ca. 3.1 eV). The

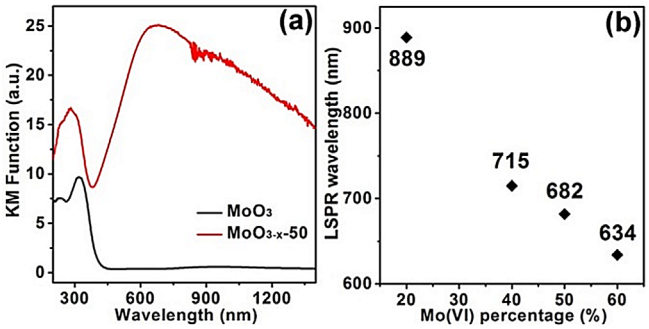

Figure 2. a) UV/Vis-NIR diffuse reflectance spectra of the MoO_{3-x}-50 sample and commercial MoO_3. b) The LSPR wavelength of the products prepared by using different ratios of Mo^{VI}/Mo^{V} in the synthesis.

MoO_{3-x}-50 sample displays a broad absorption over the entire visible-NIR wavelength range and its absorption peak is centered at 682 nm, showing a dramatic difference compared with that of MoO_3. It should be due to the new vacancy band located below the conduction-band edge of pure MoO_3 created by the introduction of oxygen vacancies, as is the case with O-deficient WO_{3-x} and TiO_{2-x}.[11a,b]

The influence of the Mo^{VI}/Mo^{V} ratio on the nanostructure and plasmonic resonances of the MoO_{3-x}-Y samples were studied (see the Supporting Information). All the MoO_{3-x}-Y samples with different Mo^{VI}/Mo^{V} ratios exhibit similar diffraction characteristics in the XRD patterns, which is indicative of the presence of a disordered amorphous phase in the samples (see the Supporting Information). MoO_{3-x}-50 and MoO_{3-x}-60 are more deeply colored than MoO_{3-x}-20 and MoO_{3-x}-40. FE-SEM observation indicates that they have granular structures with diameters of 90–200 nm except for MoO_{3-x}-60 that had a bulk morphology (see the Supporting Information). Moreover, the average particle size of the MoO_{3-x}-Y samples tends to decrease in the order of MoO_{3-x}-20 > MoO_{3-x}-40 > MoO_{3-x}-50 and this feature of the particle size change was clearly confirmed by the particle-size distribution measurements, as shown in the Supporting Information. According to this trend, the smallest nanoparticles should be observed for MoO_{3-x}-60; however, only bulk structures appeared in its SEM image (in the Supporting Information), which indicate its particles are too small to prevent aggregation arising from their high surface-to-

volume ratio.[12a] The bulk structures of MoO_{3-x}-60 can be considered as aggregates of small particles strongly joined together.[12b] The UV-visible diffraction spectra of MoO_{3-x}-Y (Supporting Information) show that all the MoO_{3-x}-Y samples have absorptions up to approximately 400 nm, consistent with the bandgap absorption edge of MoO_3 at approximately 3.1 eV. Moreover, the corresponding LSPR wavelength of MoO_{3-x}-Y samples is blueshifted from 889 to 634 nm with an increase of the amount of Mo^{VI} added during their preparation process, which follows the order of MoO_{3-x}-20 > MoO_{3-x}-40 > MoO_{3-x}-50 > MoO_{3-x}-60 (Figure 2b).

To clarify the molybdenum oxidation state and stoichiometry of MoO_{3-x}-Y, the samples were characterized by using X-ray photoelectron spectroscopy (XPS). Figure 3a shows the high-resolution Mo 3d XPS spectra of MoO_{3-x}-50 and the commercial MoO_3 sample. For the commercial MoO_3 sample, two

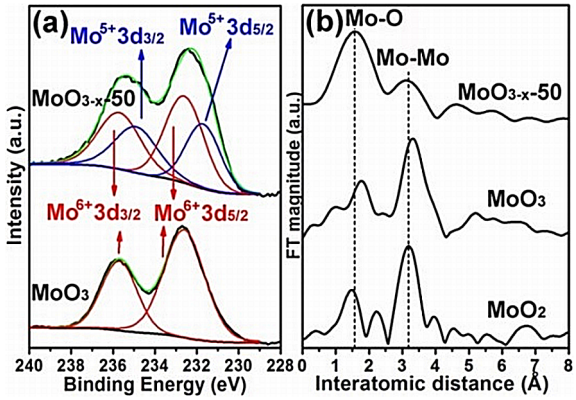

Figure 3. a) Mo 3d XPS spectra of the as-prepared MoO_{3-x}-50 and commercial MoO_3 samples. b) FT-EXAFS spectra for the MoO_{3-x}-50 and the Mo oxide references (commercial MoO_3 and MoO_2).

peaks at the binding energies of 232.6 and 235.7 eV were attributed to the $3d_{5/2}$ and $3d_{3/2}$ of Mo^{6+}, respectively.[13] In the case of MoO_{3-x}-50, the binding energy of Mo $3d_{5/2}$ and Mo $3d_{3/2}$ can be observed at 232.4 and 235.3 eV, respectively, showing a shift to lower binding energies compared with that of MoO_3. These two peaks can be fitted into two sets of peaks, which indicate the appearance of the Mo^{5+} oxidation state in MoO_{3-x}-50. The peaks at 232.6 and 235.7 eV were ascribed to Mo^{6+}, while those centered at 231.7 and 234.9 eV were assigned to Mo^{5+} ions.[13] By calculating the ratio of the peak area between Mo^{6+} and Mo^{5+}, these two kinds of cations account for 60.1 and 39.9% of the total Mo atoms in the MoO_{3-x}-50 nanoparticles, respectively. Therefore, the average oxidation state of Mo is about 5.60, further confirming the existence of oxygen vacancies that lead to plasmon absorption in the visible and NIR region. Moreover, the intensities of the Mo^{5+} peaks become stronger with the increase of the amount of Mo^{V} added during preparation processes, and the total valence state of Mo in the samples increases in the order of MoO_{3-x}-20 < MoO_{3-x}-40 < MoO_{3-x}-50 < MoO_{3-x}-60 (see the Supporting Information). This indicates that the chemical composition of the obtained samples can be tailored by adjusting the ratio Mo^{VI}/Mo^{V}. In addition, the Fourier transform curves of the k^3-weighted extended X-ray absorption fine structure (EXAFS) of the studied samples are shown in Figure 3b and in the Supporting Information. The peaks near 1.5 Å are due to the Mo–O bond in the molybdenum oxides[11c] and the obtained Mo–O distance of MoO_{3-x}-50 (1.56 Å) is longer than that of MoO_2 (1.47 Å) but shorter than that of MoO_3 (1.78 Å) (Figure 3b), which indicates the existence of low-valence Mo species. Similarly, the Mo–O distances of other MoO_{3-x}-Y (Y = 20, 40 and 60) samples are also in the range of 1.47–1.78 Å (see the Supporting Information).

To investigate the catalytic activities of the MoO_{3-x}-Y nanoparticles prepared with different ratios of Mo^{VI}/Mo^{V}, we conducted hydrogen production through the dehydrogenation of ammonia borane (NH_3BH_3) catalyzed by the MoO_{3-x}-Y samples. The dehydrogenation of ammonia borane to produce H_2 can be described by Equation (1):

$$H_3NBH_3 + 2\,H_2O \rightarrow 3\,H_2 + NH_4^+ + BO_2^- \quad (1)$$

NH_3BH_3 is of great interest for hydrogen storage because of its lightweight, room-temperature stability, and high storage capability, thus the NH_3BH_3 hydrolysis is a promising method for releasing H_2.[14] In this work, all the catalytic reactions were conducted under an Ar atmosphere at room temperature (25 °C) and similar conditions were utilized. The added amounts of NH_3BH_3, H_2O, and MoO_{3-x}-Y were fixed to 20 μmol, 5 mL, and 20 mg in the photocatalytic reactions, respectively. No catalytic activity was observed in the blank test, even under visible-light irradiation, which shows the inherent stability of NH_3BH_3 in water. The catalytic performance of the different samples was first measured in the dark. Both of the MoO_3 and MoO_{3-x}-50 catalysts exhibited H_2 production activity from aqueous NH_3BH_3 under the dark conditions (Figure 4a). After reacting for 70 minutes in the dark, about 41.2 μmol of H_2 was generated over the MoO_{3-x}-50 sample, whose initial reaction rate (H_2 yield in initial 10 min: 2.10 μmol min^{-1}) was faster than that of commercial MoO_3 (0.74 μmol min^{-1}). Under visible-light irradiation ($\lambda > 420$ nm), the hydrogen evolution of MoO_{3-x}-50

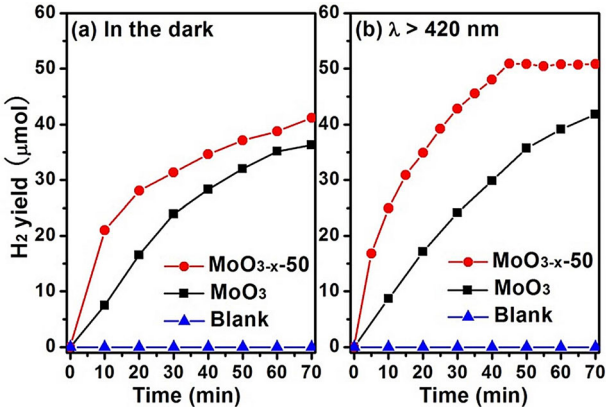

Figure 4. Hydrogen generation from aqueous NH_3BH_3 solution in the presence of different molybdenum oxide photocatalysts a) in the dark and b) under visible-light irradiation.

was finished in 45 minutes and its H_2 yield reached a maximum (50.8 μmol), as shown in Figure 4b. Therefore, the catalytic activity of MoO_{3-x}-50 was enhanced owing to the strong LSPRs absorption of MoO_{3-x}-Y nanoparticles in the visible-light and NIR region. Moreover, the initial hydrogen evolution rate of MoO_{3-x}-50 nanoparticles can reach 2.49 μmol min^{-1}, which is about 2.9-fold higher than that of MoO_3 with a photocatalytic H_2-production rate of 0.87 μmol min^{-1}. A detailed representation of the initial reaction rate and H_2 yield of all the catalysts is summarized in the Supporting Information. Under visible-light irradiation ($\lambda > 420$ nm), the initial H_2 generation rates from NH_3BH_3 are in the order of MoO_{3-x}-50 > MoO_{3-x}-20 > MoO_{3-x}-40 > MoO_{3-x}-60 > MoO_3. Among the studied MoO_{3-x}-Y samples, MoO_{3-x}-50 showed the highest H_2 evolution yield, whereas MoO_{3-x}-60 showed the shortest reaction completion time (40 min). An additional large-scale experiment demonstrated that the turn-over number (TON) exceeds 3.5 (see the Supporting Information), which provides evidence that MoO_{3-x}-50 works as a catalyst. To the best of our knowledge, the present work reports for the first time on the room-temperature synthesis of plasmonic semiconductor materials with enhanced visible-light catalytic activities for hydrogen generation from NH_3BH_3 hydrolysis.

During the H_2 generation process, photoexcitation can create thermal energy and the water temperature was found to increase from 25 to 40 °C. To determine the influence of the photothermal effect on H_2 generation, the H_2-generation experiment was carried out at 40 °C in the dark (see the Supporting Information). The initial H_2 generation rate was found to be 2.10 μmol min^{-1}, which was increased slightly relative to the yield at room temperature (25 °C, 2.20 μmol min^{-1}). Compared with the initial rate under visible-light irradiation (2.49 μmol min^{-1}), thermal catalysis has a limited effect on H_2-generation enhancement (ca. 24.6%), which indicates the critical role of LSPR excitation from MoO_{3-x}-Y nanoparticles.

To explore the wavelength dependence of the photocatalytic enhancement, several control experiments were carried out by using monochromatic light ($\lambda = 440$ or 480 nm) and a red light-emitting diode (LED) lamp ($\lambda = 627$ nm) as light sources (see the Supporting Information). The initial H_2-generation rate increases with the wavelength increase of the incident light and the light with 627 nm wavelength exhibits the most effective photocatalytic effect among all these three cases, which is consistent with the light absorption of MoO_{3-x}-50 in the visible-light region. It suggests that the enhancement of H_2 generation mainly originates from the plasmonic properties of MoO_{3-x}-Y nanoparticles.[15,16]

To provide more evidence that the H_2 production is enhanced by the LSPR adsorption of MoO_{3-x}-Y nanoparticles, $NaHCO_3$ was introduced as a positive-charge scavenger into the H_2-generating system during the catalytic reactions. Under visible-light irradiation ($\lambda > 420$ nm), charge separation can be initiated by the LSPR plasma oscillation of MoO_{3-x}-Y nanoparticles. The HCO_3^- ions can adsorb on the catalyst surface and react with positive charges generated on the plasmonic catalyst, so the H_2-generation enhancement is markedly depressed in the presence of $NaHCO_3$.[17] Moreover, the H_2-generation activity is reduced more significantly under light irradiation than the case of H_2 generated in the dark (see the Supporting Information), which indicates that the plasmon-induced charge separation and the activation of NH_3BH_3 are significantly inhibited. Besides the photocatalytic activity, the catalyst stability is also important. The cycling catalytic performance of MoO_{3-x}-50 has been investigated to check its stability. As shown in the Supporting Information, a slight activity decrease was observed during three successive cycles. However, XRD patterns and UV-visible-NIR diffuse reflectance spectra of MoO_{3-x}-50 before and after the cyclic stability tests show similar results. This indicates the structural and chemical stability of the as-prepared MoO_{3-x}-Y nanoparticles, which suggests its potential application in visible-light catalytic hydrogen production.

In conclusion, the MoO_{3-x} nanoparticles were prepared at room temperature, and exhibited strong plasmonic absorption in the visible light and near-infrared regions. The catalytic results indicate that such MoO_{3-x} structures can enhance visible-light-induced H_2 production from NH_3BH_3 hydrolysis due to its LSPR properties. The present study provides a useful and convenient strategy for the fabrication of plasmonic semiconductor materials for practical solar energy utilization and LSPR-enhanced hydrogen production.

Acknowledgements

The authors acknowledge financial support from the China Scholarship Council. This work was also supported by China Postdoctoral Science Foundation (2014M552247), the strategic China–Japan research cooperative program 2012 from JST, and the Natural Science Foundation of China (NSFC, 41425015).

Keywords: green chemistry · molybdenum oxide · nanoparticles · photochemistry · surface plasmon resonance

[1] a) N. S. Lewis, D. G. Nocera, *Proc. Natl. Acad. Sci. USA* **2006**, *103*, 15729–15735; b) M. Z. Jacobson, *Energy Environ. Sci.* **2009**, *2*, 148–173.
[2] a) B. Johnston, M. C. Mayo, A. Khare, *Technovation* **2005**, *25*, 569–585; b) M. Ball, M. Wietschel, *Int. J. Hydrogen Energy* **2009**, *34*, 615–627.
[3] a) D. M. Fabian, S. Hu, N. Singh, F. A. Houle, T. Hisatomi, K. Domen, F. E. Osterloh, S. Ardo, *Energy Environ. Sci.* **2015**, *8*, 2825–2850; b) D. B. Levin, P. L. Lawrence, M. Love, *Int. J. Hydrogen Energy* **2004**, *29*, 173–185; c) M. Ni, M. K. H. Leung, D. Y. C. Leung, K. Sumathy, *Renewable Sustainable Energy Rev.* **2007**, *11*, 401–425.
[4] P. Zhang, T. Wang, J. Gong, *Adv. Mater.* **2015**, *27*, 5328–5342.
[5] a) M. Rycenga, C. M. Cobley, J. Zeng, W. Y. Li, C. H. Moran, Q. Zhang, D. Qin, Y. N. Xia, *Chem. Rev.* **2011**, *111*, 3669–3712; b) H. J. Chen, L. Shao, Q. Li, J. F. Wang, *Chem. Soc. Rev.* **2013**, *42*, 2679–2724; c) K. Mori, M. Kawashima, M. Che, H. Yamashita, *Angew. Chem. Int. Ed.* **2010**, *49*, 8598–8601; *Angew. Chem.* **2010**, *122*, 8780–8783.
[6] a) V. J. Babu, S. Vempati, T. Uyar, S. Ramakrishna, *Phys. Chem. Chem. Phys.* **2015**, *17*, 2960–2986; b) H. Cheng, X. Qian, Y. Kuwahara, K. Mori, H. Yamashita, *Adv. Mater.* **2015**, *27*, 4616–4621; c) Z. Zhang, Z. Wang, S.-W. Cao, C. Xue, *J. Phys. Chem. C* **2013**, *117*, 25939–25947; d) Z. Zheng, T. Tachikawa, T. Majima, *J. Am. Chem. Soc.* **2014**, *136*, 6870–6873; e) X. Zhou, Y. Huang, W. Xing, C. Liu, J. Liao, T. H. Lu, *Chem. Commun.* **2008**, 3540–3542.
[7] a) Z. Lou, Q. Gu, L. Xu, Y. Liao, C. Xue, *Chem. Asian J.* **2015**, *10*, 1291–1294; b) M. Lee, J. U. Kim, K. J. Lee, S. H. Ahn, Y.-B. Shin, J. Shin, C. B. Park, *ACS Nano* **2015**, *9*, 6206–6213.

[8] a) Y. Zhao, C. Burda, *Energy Environ. Sci.* **2012**, *5*, 5564 – 5576; b) G. V. Naik, V. M. Shalaev, A. Boltasseva, *Adv. Mater.* **2013**, *25*, 3264 – 3294.
[9] a) T. R. Gordon, T. Paik, D. R. Klein, G. V. Naik, H. Caglayan, A. Boltasseva, C. B. Murray, *Nano Lett.* **2013**, *13*, 2857 – 2863; b) R. Buonsanti, A. Llordes, S. Aloni, B. A. Helms, D. J. Milliron, *Nano Lett.* **2011**, *11*, 4706 – 4710; c) J. M. Xu, L. Li, S. Wang, H. L. Ding, Y. X. Zhang, G. H. Li, *CrystEngComm* **2013**, *15*, 3296 – 3300.
[10] a) J. M. Luther, P. K. Jain, T. Ewers, A. P. Alivisatos, *Nat. Mater.* **2011**, *10*, 361 – 366; b) D. Dorfs, T. Härtling, K. Miszta, N. C. Bigall, M. R. Kim, A. Genovese, A. Falqui, M. Povia, L. Manna, *J. Am. Chem. Soc.* **2011**, *133*, 11175 – 11180.
[11] a) M. Wajid Shah, Y. Zhu, X. Fan, J. Zhao, Y. Li, S. Asim, C. Wang, *Sci. Rep.* **2015**, *5*, 15804; b) K. Manthiram, A. P. Alivisatos, *J. Am. Chem. Soc.* **2012**, *134*, 3995 – 3998; c) H. Cheng, T. Kamegawa, K. Mori, H. Yamashita, *Angew. Chem. Int. Ed.* **2014**, *53*, 2910 – 2914; *Angew. Chem.* **2014**, *126*, 2954 – 2958; d) Q. Huang, S. Hu, J. Zhuang, X. Wang, *Chem. Eur. J.* **2012**, *18*, 15283 – 15287.
[12] a) W. Wu, Q. He, C. Jiang, *Nanoscale Res. Lett.* **2008**, *3*, 397 – 415; b) H. Nagai, K. Kataoka, J. Akimoto, T. Sotokawa, Y. Kumashiro, *Electrochemistry* **2015**, *83*, 834 – 836.
[13] a) M. Vasilopoulou, A. M. Douvas, D. G. Georgiadou, L. C. Palilis, S. Kennou, L. Sygellou, A. Soultati, I. Kostis, G. Papadimitropoulos, D. Davazoglou, P. Argitis, *J. Am. Chem. Soc.* **2012**, *134*, 16178 – 16187; b) M. M. Y. A. Alsaif, M. R. Field, B. J. Murdoch, T. Daeneke, K. Latham, A. F. Chrimes, A. S. Zoolfakar, S. P. Russo, J. Z. Ou, K. Kalantar-zadeh, *Nanoscale* **2014**, *6*, 12780 – 12791; c) M. M. Y. A. Alsaif, K. Latham, M. R. Field, D. D. Yao, N. V. Medehkar, G. A. Beane, R. B. Kaner, S. P. Russo, J. Z. Ou, K. Kalantar-zadeh, *Adv. Mater.* **2014**, *26*, 3931 – 3937.
[14] a) B. C. H. Steele, A. Heinzel, *Nature* **2001**, *414*, 345 – 352; b) K. Mori, P. Verma, R. Hayashi, K. Fuku, H. Yamashita, *Chem. Eur. J.* **2015**, *21*, 11885 – 11893; c) A. D. Sutton, A. K. Burrell, D. A. Dixon, E. B. Garner, III, J. C. Gordon, T. Nakagawa, K. C. Ott, J. P. Robinson, M. Vasiliu, *Science* **2011**, *331*, 1426 – 1429.
[15] K. Fuku, R. Hayashi, S. Takakura, T. Kamegawa, K. Mori, H. Yamashita, *Angew. Chem. Int. Ed.* **2013**, *52*, 7446 – 7450; *Angew. Chem.* **2013**, *125*, 7594 – 7598.
[16] S. Linic, P. Christopher, D. B. Ingram, *Nat. Mater.* **2011**, *10*, 911 – 921.
[17] C. Hu, T. Peng, X. Hu, Y. Nie, X. Zhou, J. Qu, H. He, *J. Am. Chem. Soc.* **2010**, *132*, 857 – 862.

Manuscript received: June 1, 2016
Revised: June 27, 2016
Final Article published: ■■ ▮▮, 0000

COMMUNICATION

Photochemistry

*Jiayuan Shi, Yasutaka Kuwahara, Meicheng Wen, Miriam Navlani-García, Kohsuke Mori, Taicheng An, Hiromi Yamashita**

■■ – ■■

Room-Temperature and Aqueous-Phase Synthesis of Plasmonic Molybdenum Oxide Nanoparticles for Visible-Light-Enhanced Hydrogen Generation

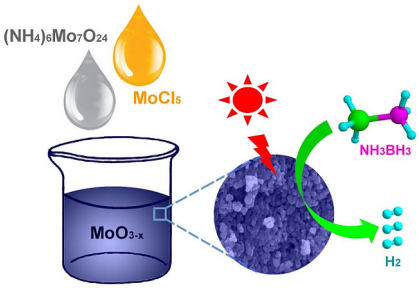

Bright idea: Plasmonic MoO_{3-x} nanoparticles were fabricated at room temperature without the use of reductants. The obtained MoO_{3-x} exhibited enhanced visible-light catalytic activity toward hydrogen generation from ammonia borane (see figure).